JCTC Journal of Chemical Theory and Computation

Article

pubs.acs.org/JCTC

# Reliable Quantum Chemical Prediction of the Localized/Delocalized Character of Organic Mixed-Valence Radical Anions. From Continuum Solvent Models to Direct-COSMO-RS

Manuel Renz,[†] Martin Kess,[†] Michael Diedenhofen,[‡] Andreas Klamt,[‡] and Martin Kaupp*[,†]

[†]Technische Universität Berlin, Institut für Chemie, Theoretische Chemie, Sekr. C7, Strasse des 17. Juni 135, 10623 Berlin, Germany

[‡]COSMOlogic GmbH & Co. KG, Burscheider Strasse 515, D-51381 Leverkusen, Germany

Supporting Information

**ABSTRACT:** A recently proposed quantum-chemical protocol for the description of the character of organic mixed-valence (MV) compounds, close from both sides to the localized/delocalized borderline, is evaluated and extended for a series of dinitroaryl radical anions **1**−**6**. A combination of global hybrid functionals with exact-exchange admixtures of 35% (BLYP35) or 42% (BMK) with appropriate solvent modeling allows an essentially quantitative treatment of, for example, structural symmetry-breaking in Robin/Day class II systems, thermal electron transfer (ET) barriers, and intervalence charge-transfer (IV-CT) excitation energies, while covering also the delocalized class III cases. Global hybrid functionals with lower exact-exchange admixtures (e.g., B3LYP, M05, or M06) provide a too delocalized description, while functionals with higher exact-exchange admixtures (M05-2X, M06-2X) provide a too localized one. The B2PLYP double hybrid gives reasonable structures but far too small barriers in class II cases. The CAM-B3LYP range hybrid gives somewhat too high ET barriers and IV-CT energies, while the range hybrids ωB97X and LC-BLYP clearly exhibit too much exact exchange. Continuum solvent models describe the situation well in most aprotic solvents studied. The transition of 1,4-dinitrobenzene anion **1** from a class III behavior in aprotic solvents to a class II behavior in alcohols is not recovered by continuum solvent models. In contrast, it is treated faithfully by the novel direct conductor-like screening model for real solvents (D-COSMO-RS). The D-COSMO-RS approach, the TURBOMOLE implementation of which is reported, also describes accurately the increased ET barriers of class II systems **2** and **3** in alcohols as compared to aprotic solvents and can distinguish at least qualitatively between different aprotic solvents with identical or similar dielectric constants. The dominant role of the solvent environment for the ET character of these MV radical anions is emphasized, as in contrast to some previous computational suggestions essentially all of the present systems have delocalized class III character in the gas phase. The present approach allows accurate estimates from the gas phase to aprotic and protic solvent environments, without the need for explicit ab initio molecular dynamics simulations, and without artificial constraints.

## INTRODUCTION

Electron transfer (ET) processes are of fundamental importance in many fields, from molecular, heterogeneous, or biocatalysis to molecular electronics, quantum computing, conductivity, energy transduction, and so on. In this context, mixed-valence (MV) compounds play a key role.[1−4] They provide the prototypical intramolecular, isoenthalpic ET and are thus basic models for more complex intra- and intermolecular processes. At the same time, many MV compounds are of potential technological or biochemical interest on their own. While the interest in this field had originally been stimulated by MV transition-metal complexes such as the Creutz−Taube ion, the past 10−15 years have provided tremendous progress in the field of organic compounds that may be viewed as MV systems.[5,6] Some of their advantages are the relatively straightforward synthesis and modification of such molecules, their often high thermal and kinetic stabilities, and the sometimes easier analysis of their UV/vis or NIR spectra. In fact, the peculiar EPR spectroscopic behavior of dinitroaryl radical anions, the central species of this Article, has been studied in detail since the early 1960s, even before the very notion of mixed-valency had been discussed.[7−18]

In the classification scheme of Robin and Day[19] (Figure 1), MV systems are divided into three general classes, ranging from a fully trapped, localized system with negligible electronic coupling between the diabatic states of the two redox centers (class I) to valence-trapped systems, where the electronic coupling $2H_{ab}$ between the diabatic states is non-negligible but less than the Marcus reorganization energy $\lambda$ (leading to a double-minimum adiabatic ground-state potential-energy surface; class II), to fully valence-delocalized systems ($2H_{ab} > \lambda$; class III; no classical barrier for thermal electron transfer, see Figure 1). The transition between classes II and III has been of particular interest in many studies, as the fundamentals of ET processes differ for the two cases. The still growing toolbox of organic as well as transition-metal MV compounds has recently contributed to the increasing observation of particularly interesting systems that are close to the class II/III boundary.[3,20−22] When the thermal electron transfer barrier

Received: June 28, 2012
Published: September 5, 2012

   dx.doi.org/10.1021/ct300545x | J. Chem. Theory Comput. 2012, 8, 4189−4203

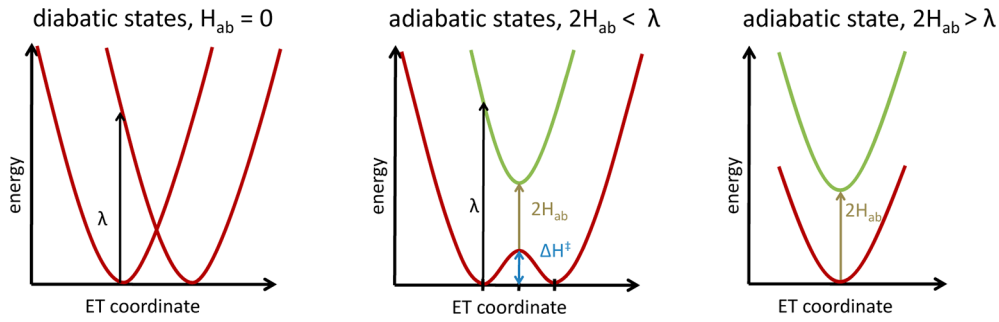


**Figure 1.** Robin/Day classification of MV systems. Left: Class I, diabatic states, no coupling, fully localized. Middle: Class II, adiabatic states, intermediate coupling, partly localized. Right: Class III, adiabatic states, strong coupling, fully delocalized.

becomes small, approaching thermal energies, experimental distinction between class II and class III systems is very difficult, as the different time scales of various spectroscopic techniques (UV/vis, NIR, IR, EPR, NMR) and of the different motions of the system (intramolecular reorganization, fast and slow solvent reorganization modes) may lead to seemingly conflicting information.[3] The characterization of the ET processes is typically based on parameters extracted from these spectroscopic measurements via suitable model theories (e.g., the generalized Mulliken−Hush theory, two- and three-state models, etc.),[23−27] and thus the ET near the localized/delocalized borderline remains incompletely understood.

A purely theoretical characterization of the adiabatic ground- and excited-state potential energy surfaces of mixed-valence systems by quantum-chemical methodology is highly desirable, as the relevant ET parameters may then be obtained without reference to simplified model approaches, and without the complications arising from the interpretation of the spectroscopic data. In fact, the comparison of ET parameters computed solely by quantum chemistry with those extracted from spectroscopy should provide the ultimate reality check and a basis for deeper understanding. Until recently, such a quantum-chemical characterization of mixed-valence systems near the class II/III border had not been available. Sophisticated post-Hartree−Fock (HF) approaches that incorporate quantitatively both the crucial dynamical and the nondynamical electron correlation effects have not been applicable to MV systems of chemically relevant sizes, while also covering environmental effects (see below). While (ab initio or semiempirical) Hartree−Fock (or MCSCF) theory gives an overly localized description due to the lack (or underestimate) of Coulomb correlation,[28−30] standard density functional theory (DFT) approaches have painted a much too delocalized picture, due to self-interaction errors (alternatively termed fractional-charge or delocalization errors[22,31]). Moreover, as most MV systems are studied experimentally in polar solvents or in the solid state, and charge localization is strongly influenced by these environments, the neglect of environmental effects in most ground-state structure optimizations has biased the calculations strongly toward a delocalized character [inclusion of solvent effects in subsequent single-point time-dependent density functional theory (TDDFT) calculations of excitation spectra is not sufficient to remedy this problem]. Some calculations on MV systems near the class II/III borderline that used DFT functionals with high constant exact-exchange admixtures or range-separated hybrids, but that neglected environmental effects in the structure optimizations, may have provided a distorted picture as well, or possibly gave the (qualitatively) right answer for the wrong reason (see below). Constrained DFT (CDFT) approaches,[32] which force a localized or delocalized character by adding deliberately certain terms to the Hamiltonian, have recently been used as well. However, they lack predictive power, as the localized/delocalized character is an input parameter. Before our recent work (see below), only a few calculations on MV systems included solvent effects in the structure optimization.[33−35] We will refer to these further below.

We have recently suggested[36] a general computational protocol for the treatment of organic MV systems near the class II/III border, which is based on ground-state structure optimizations using a nonstandard global hybrid functional with an exact-exchange admixture of 35% (BLYP35), together with continuum solvent models to treat the environmental effects, followed by TDDFT calculations of the intervalence charge-transfer (IV-CT) excitations using the same functional and solvent model. Careful validation and calibration[36,37] of the approach for an extended set of MV bis-triarylamine radical cations, and for some unsymmetrical, neutral arylamine-arylmethyl radicals, have provided (a) an unprecedentedly fine distinction of localization/delocalization of the ground state for systems near the class II/III borderline, (b) realistic barriers for thermal electron transfer in class II systems, and (c) rather accurate IV-CT excitation energies with reasonable trends in the oscillator strengths. Additionally, ground- and excited-state dipole moments, as well as EPR hyperfine couplings, could be reproduced reliably. Notably, the choice of solvent turned out to be crucial for the character of a given system and is an intrinsic property of an overall MV system consisting of the molecule/ion and its environment.[36,37]

Here, we extend the approach fundamentally and validate various schemes for a set of six dinitroaromatic radical anions **1**−**6** (Chart 1). This choice allows not only the evaluation of computational challenges related to the negative charge (e.g., larger specific solvation effects and basis set requirements) and of quite different redox centers as compared to the triarylamine systems studied previously. The much smaller size of these anions as compared to the bulky radical cations of the previous investigations permits a much wider range of computational approaches to be studied: (i) In previous work, we used mostly a locally modified version of the TURBOMOLE code for the structure optimizations. This program allows fast calculations on relatively large systems but so far exhibits a relatively limited range of DFT functionals. Here, we employ in addition the Gaussian 09 program. This enables us to evaluate also a range of popular, highly parametrized meta-GGA hybrid functionals (M05, M06, M05-2X, M06-2X, BMK), three range-separated hybrids (CAM-B3LYP, ωB97X, LC-BLYP), and a double hybrid (B2PLYP). (ii) Most importantly, we have gone beyond

**Chart 1. Six Dinitroaromatic Radical Anions Studied**

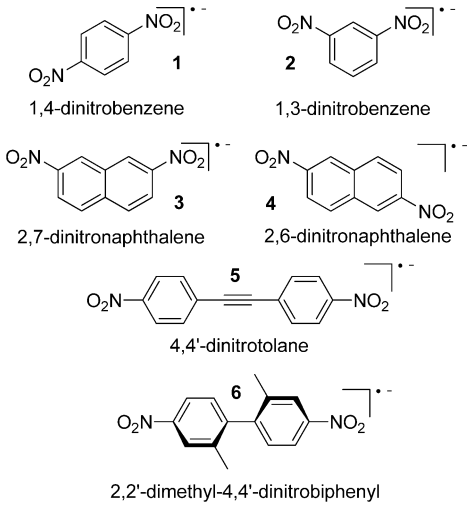


the previously used dielectric continuum solvent models by using the direct COSMO for real solvents (D-COSMO-RS) approach.[38] Except for a recent report on electronic *g*-tensors of nitroxide radicals,[38] this is the first detailed evaluation of D-COSMO-RS, and we report here for the first time on the TURBOMOLE implementation of D-COSMO-RS. A number of previous computational studies have dealt with some of the present dinitroaromatic radical anions (mainly **1**, **2**, and **3**).[33−35,39−43] We will refer to some of these calculations further below.

## MOLECULAR TEST SET OF DINITROAROMATIC RADICAL ANIONS

Chart 1 shows the six dinitroaromatic radical anions studied in this work. The two nitro substituents are the redox centers, connected by aromatic bridges. Some of these anions are among the earliest MV systems studied in the 1960s,[7−18] in particular by ESR spectroscopy, and they cover the range from class II to class III of the Robin/Day scheme while remaining sufficiently close to the borderline to be a challenge for standard quantum-chemical treatments.

The radical anion of 1,4-dinitrobenzene, **1**, is a class III system in aprotic solvents, consistent with strong electronic coupling for a Kekulé substitution pattern, that is, for an odd number of bonds between the two nitrogen atoms. **1** does not exhibit alternating line-broadening effects in ESR in aprotic solvents and has narrow, intense low-energy optical bands with vibrational structure with maxima at 10 820 and 11 000 $cm^{-1}$ in dimethylformamide (DMF) and in acetonitrile (MeCN), respectively.[44,45] Lü et al. showed by X-ray crystallography, and by spectroscopy in solution, that strong ion pairing can lead to an asymmetrical structure of **1**, whereas use of cryptands to prevent ion pairing keeps the system delocalized even in the solid state.[46] Preliminary calculations (Figure S3 in the Supporting Information) confirm that close ion pairing can distort **1** when the counterion is placed near one of the nitro groups. Given that the above-mentioned spectroscopic data in aprotic solution all suggest class III character, strong ion pairing under these conditions is unlikely. However, due to hydrogen bonding (see below), the system becomes class II on the ESR time scale in alcohol solvents even up to near room temperature, with estimated thermal electron transfer (ET) barriers ($\Delta H^{\ddagger}$) between 22 and 36 kJ $mol^{-1}$, depending on the specific alcohol solvent.[47] The 2,6-dinitronaphthalene radical anion **4** is also a class III system in aprotic solvents,[33,44] with a narrow, intense IV-CT band in DMF.

In contrast, the radical anion of 1,3-dinitrobenzene, **2**, has a non-Kekulé substitution pattern, with an even number of bonds between the nitrogen atoms. It exhibits class II character already in polar aprotic solvents like MeCN or DMF, with alternating ESR line-broadening, broad intervalence charge transfer (IV-CT) bands, and ESR-derived thermal ET barriers of about 22 kJ $mol^{-1}$ in MeCN or DMF.[33,45] These values have been obtained after electrochemical reduction. Measurements in the presence of cryptand to suppress ion pairing gave ET barriers (at 298 K) of ca. 26 kJ $mol^{-1}$ in MeCN and of ca. 16 kJ $mol^{-1}$ ion DMF.[48] This suggests again that ion pairing, while overall non-negligible, does not affect the ET barriers in these environments to an extent that would invalidate the present calculations that neglect the influence of counterions. Within the general accuracy of the approach, this holds also largely for the other systems studied here. In alcohol solvents, barriers of about 43 kJ $mol^{-1}$ have been measured for **2**, enhanced by hydrogen bonding (here, ion pairing is expected to play an even smaller role).[47,49,50]

Similarly, the radical anion of 2,7-dinitronaphthalene, **3**, is on the class II side already in aprotic solvents (in fact, **3** is the clearest class II case in this study, see below), with broad IV-CT bands in MeCN and in DMF.[33] According to ESR studies, ET barriers are about 18 kJ $mol^{-1}$ in MeCN and of ca. 12−13 kJ $mol^{-1}$ in DMF and in hexamethylphosphoramide (HMPA).[51] The corresponding barriers in alcoholic solvents are around 50 kJ $mol^{-1}$.[52]

The 4,4′-dinitrotolane-bridged system **5** is of particular interest by being extremely close to the class II/III transition in aprotic solvents.[53] Optical spectra and resonance Raman spectra suggest that delocalized and localized forms of the radical anion coexist, with the predominance of one over the other depending on the solvent.[54] In solvents with presumably low solvent reorganization energies, $\lambda_s$, such as tetrahydrofuran (THF) or HMPA,[55,56] typical charge-delocalized spectra dominate. A small fraction of localized spectra persists, however, even when an excess of cryptand[2.2.2] is added during reduction to minimize ion pairing. In these solvents, the maximum in the absorption band of the delocalized species is at 5860 $cm^{-1}$. In higher $\lambda_s$-solvents, typical charge-localized spectra with broad IV-CT bands dominate. The band maxima range from 9560 $cm^{-1}$ in DMF and 10 800 $cm^{-1}$ in dichloromethane (DCM) to 11 300 $cm^{-1}$ in MeCN. ESR-based ET barriers for the localized species are $\Delta H^{\ddagger}$ = 11.3(±1.7) kJ $mol^{-1}$ in MeCN, 13.8(±1.88) kJ $mol^{-1}$ in DMF, and 11.5(±0.88) kJ $mol^{-1}$ in DCM.[51]

In the radical anion of 2,2′-dimethyl-4,4′-dinitrobiphenyl, **6**, the presence of two methyl groups leads to a twisting of the two phenyl rings relative to each other.[51] The resulting reduced overlap of the $\pi$-orbitals is expected to decrease electronic coupling and to favor a class II situation. This was confirmed by optical and ESR spectra in several aprotic solvents (e.g., MeCN, DMF, or DCM). Broad IV-CT bands are observed in DMF, DCM, and MeCN, whereas the spectra in HMPA are consistent with both class III and class II species being present.[51] The ESR-based ET barriers $\Delta H^{\ddagger}$ are 8.8(±1.25) kJ $mol^{-1}$ in MeCN, 13.8(±1.67) kJ $mol^{-1}$ in DMF, and 4.2(±0.84) kJ $mol^{-1}$ in DCM.[51]

## COMPUTATIONAL DETAILS

**Program Versions, Continuum Solvent Models, and Basis Sets.** In our previous studies of organic mixed-valence systems, we had mainly employed a version of the TURBOMOLE 5.10[57] code, locally modified to allow variation of the exact-exchange admixture in global hybrid functionals, for the ground-state structure optimizations, and the Gaussian 03 (G03)[58] code for subsequent TDDFT calculations of excitation energies and oscillator strengths. This use of two codes was mainly due to differences in computational efficiency and in the solvent models implemented: while TURBOMOLE was more suitable for the many ground-state optimizations with different exact-exchange admixtures and solvents, its implementation of the conductor-like-screening (COSMO) solvent model did not account for nonequilibrium solvation in the TDDFT calculations, whereas the CPCM solvent model in G03 does. This affected the computed IV-CT excitation energies substantially, in particular for class II systems, and the G03/CPCM results were closer to experiment (negligible differences arose in gas-phase calculations). Meanwhile, newer versions of both codes have appeared, TURBOMOLE 6.3[59] (also locally modified), and Gaussian 09 (G09),[60] with updates to the solvent models. In particular, a separation of fast and slow solvent modes in TDDFT is now also available in TURBOMOLE.

In the present study, we focus on these more recent versions for the dinitroaromatic radical anions, and we have evaluated the differences from the previous versions in detailed test calculations (mainly described in Supporting Information, Tables S1−S4). The relatively small sizes of the present MV systems have allowed extensive structure optimizations with both codes and various approaches, and some of the results will be compared throughout this study. We report results with the modified TURBOMOLE 6.3 mainly in context of D-COSMO-RS[61] calculations and with Gaussian 09 mainly for evaluating a wider range of functionals (see below).

In the Gaussian calculations, the CPCM version[62,63] of the polarizable continuum (PCM) solvent model has been employed, as this is closest to the COSMO *ansatz* used in TURBOMOLE (previous tests using the IEFPCM model led to negligible changes[36]). A main change from Gaussian 03 to Gaussian 09 is the use of the continuous surface charge formalism.[64,65] Furthermore, in the construction of the cavity, the United Atom Topological Model (UA0) has been replaced by UFF radii, which treat the hydrogen atoms explicitly (this makes the Gaussian 09 and TURBOMOLE implementations more similar, even if there are still some deviations in the atomic radii used for the cavity construction; see Table S1). In the subsequent TDDFT calculations, Gaussian uses so-called "non-equilibrium solvation", where only the fast solvent modes are included in the linear response part. In TURBOMOLE 6.3, a similar division is now employed.[66,67] Table S5 provides some relevant dielectric constants and refractive indices.

Near the critical values of exact-exchange ($E_{xx}$) admixture $a$, where symmetry breaking occurs, the outcome of the ground-state structure optimizations depended sometimes on whether we used a symmetrical or unsymmetrical starting structure. Next, different unsymmetrical ($C_1$) and symmetrical (typically $C_2$, $C_s$, or $C_i$) starting structures have been evaluated, and the validity of a given structure was evaluated energetically.

Reported computational thermal electron transfer (ET) barriers, $\Delta H^{\ddagger}$, have been obtained as follows: neither zero-point vibrational corrections nor thermal corrections have been applied to the internal energies of the asymmetrical minima and the symmetrical transition-state structures. Note, however, that the various solvent models do include solvent thermal effects (and even some entropic contributions). We estimate that these approximations cause uncertainties in the computed activation enthalpies of at least 5 kJ mol$^{-1}$. This should be kept in mind when comparing to the ESR-based values (which exhibit their own intrinsic errors, see below). In selected cases, the character of the optimized stationary points has been evaluated by harmonic vibrational frequency analysis, partly to compare with resonance Raman data. In some other cases, frequencies turned out to be unreliable due to numerical aspects of the solvent models. This holds particularly for the more symmetrical ET transition states and is likely related to the segmentation of the surface charge densities. We therefore refrain from utilizing zero-point vibrational corrections.

While dipole moments for anions are not well-defined, we report them with respect to the center of charge. No experimental data are available anyhow, but the dipole moments provide a very useful indicator for localization/delocalization, in particular when the delocalized structure features zero dipole moment.

TDDFT calculations of the lowest-energy electronic transitions (IV-CT bands) for both minima and transition-state structures were done with either Gaussian or TURBOMOLE, using the same type of functional and basis sets and corresponding solvent models (see above).

Our previous calculations on MV arylamine radical cation systems could rely mostly on moderate-sized SVP basis sets,[68] as basis set augmentation had only a small influence on the results.[36] However, as it is well-known that diffuse basis functions are more important for anions, we have evaluated different basis sets for the present systems. Augmentation by a set of diffuse s- and p-functions led to SVP+ basis sets (the exponents of the additional diffuse functions for the non-hydrogen atoms were obtained by dividing the smallest s- and p-exponents of the SVP basis by a factor of 3). When diffuse augmentation was restricted to only the oxygen atoms of the nitro groups, the basis is termed SVP+(O). The largest basis set used, and the one employed finally in all further calculations, was TZVP.[69]

**Functionals.** The nonstandard global hybrid functionals of our previous study use:[36,37]

$$E_{XC} = (1 - a)(E_X^{LSDA} + \Delta E_X^{B88}) + aE_X^{HF} + E_C^{LYP} \quad (1)$$

where the exact-exchange admixture $a$ was taken as a semiempirical parameter. The value $a$ = 0.35 (BLYP35 functional) turned out to be near optimum for ground-state properties, ET barriers, and IV-CT excitation energies of the previously studied organic MV systems.[36,37] The value $a$ = 0.0 corresponds to the BLYP GGA functional,[70,71] $a$ = 0.5 to the BHLYP hybrid functional.[72] The "one-parameter" functional BLYP35 is not a thermochemically optimized functional and may thus be criticized. By introducing a dependence on local kinetic energy density in highly parametrized, so-called meta-GGA global hybrids, it is possible to combine, for example, good classical barriers and thermochemistry in main group chemistry. Some examples of such optimized functionals will be evaluated in the present work. These are the BMK functional ($a$ = 0.42),[73] Truhlar's M05 ($a$ = 0.28),[74] and M06 ($a$ = 0.27),[75] as well as their "double exact-exchange variants" M05-2X ($a$ = 0.56)[76] and M06-2X ($a$ = 0.54).[75] Additionally, we evaluate also

a number of range-separated hybrids (where exact-exchange admixture depends on the interelectronic distance) available in Gaussian 09. These are CAM-B3LYP,[77] $\omega$B97X,[78] and LC-BLYP.[79] Furthermore, the double-hybrid functional B2PLYP and its dispersion corrected version, B2PLYP(D), were applied.[80] Double hybrids include an MP2-like term as part of the correlation functional, and B2PLYP includes 53% exact-exchange admixture ($a$ = 0.53). Structures were optimized with all functionals, in particular in MeCN and in DCM solvent, where necessary with both localized and delocalized starting structures, and IV-CT excitation energies were computed at the TDDFT level with the same functional and solvent.

**Direct COSMO-RS.** To go beyond the limitations of continuum solvent models, we have applied the D-COSMO-RS approach (see Introduction).[61] While COSMO is a simple continuum solvation model, which can only take into account the polarization effects of the solvents on a plain, electrostatic level, the COSMO-RS model is a statistical thermodynamics treatment of the solute−solvent interactions, based on the COSMO polarization charge densities calculated on solute and solvent molecules in a conductor ($\varepsilon = \infty$). The essential advantage of COSMO-RS over COSMO and other dielectric continuum solvation approaches is its ability to treat solute and solvent on the same quantum-chemical basis, to take into account hydrogen bonding (as well as van der Waals terms), and to treat mixtures and temperature effects. In the present context, the inclusion of well-established specific COSMO-RS hydrogen-bonding terms of the form:[81]

$$E_{HB}(\sigma, \sigma') = a_{cont} c_{HB}(T) \min[0; \min(0; \sigma_{donor} + \sigma_{HB}) \max(0; \sigma_{acceptor} - \sigma_{HB})]$$

is decisive for modified $\sigma$-potentials. $a_{cont}$ is the segment contact area, $c_{HB}(T)$ is a temperature-dependent element-specific hydrogen-bonding coefficient (as this coefficient considers also entropic contributions, $E_{HB}$ may be considered a free energy), and $\sigma_{HB}$ is an element-specific threshold surface-charge density (typically ca. 0.8−0.9 e nm$^{-2}$).

Yet in COSMO-RS the solvation thermodynamics is handled as a separate step after the quantum chemical calculations, while the latter are always only performed at $\varepsilon = \infty$. This is a significant advantage with respect to computational efficiency, especially for the treatment of mixtures. However, it prohibits the calculation of geometrical or electronic response properties of the solute in a specific solvent. The direct COSMO-RS (D-COSMO-RS) approach makes use of the specific solvent response function calculated in COSMO-RS, the so-called $\sigma$-potential, turns it into a response operator, which is only slightly more complicated than the COSMO operator itself, and uses this in the quantum chemical calculation of solute properties in the specific solvent. Because the $\sigma$-potential can be calculated for almost any solvent and solvent mixture, even at variable temperature, and because it includes hydrogen bonding and many other effects beyond the dielectric continuum approximation, D-COSMO-RS has the potential to calculate solute geometries and spectra in specific solvents.

For the relevant solvents, BP86/TZVP pregenerated $\sigma$-potentials have been obtained from the COSMOtherm program package.[82,83] Use of COSMO-RS in self-consistent DFT implementations ("direct COSMO-RS") has been pioneered by Neese, Klamt, and co-workers within the ORCA code.[84] Here, the recent implementation of the approach in the TURBOMOLE program (version 6.3) is reported and validated. More specifically, in the present work, a locally modified version 6.3 is used, which allows the use of nonstandard hybrid functionals, such as BLYP35. D-COSMO-RS results are thus reported at the BLYP35/TZVP level.

## RESULTS AND DISCUSSION

**Basis Set Effects.** Our previous work on bis-triarylamine systems used mainly moderately sized SVP basis sets, as test calculations with larger basis sets gave only relatively small modifications, both on ground-state properties and on IV-CT excitation energies. Given the negative charge of the present test systems and the charge concentration on highly electronegative nitro groups, basis set effects had to be reevaluated. Basis set effects on the ground-state structures tend to be small but non-negligible. Test calculations on the class II system **2** indicate a slightly more asymmetrical structure when going from SVP to SVP+(O) and very little change upon further augmentation (Table S4 in the Supporting Information). Consequently, the dipole moment is somewhat enhanced. The ET barrier $\Delta H^{\ddagger}$ increases from 6.4 kJ mol$^{-1}$ [SVP] to 18.6 kJ mol$^{-1}$ [SVP+(O)] and remains close to the latter value for still larger basis sets. Probably as a consequence of the slightly more distorted ground-state structure, addition of diffuse functions on oxygen increases the IV-CT excitation energy for **2**, and thus improves agreement with experiment, when using the previously validated BLYP35 functional and suitable continuum solvent models for MeCN (Figure 2, cf. Table S4).

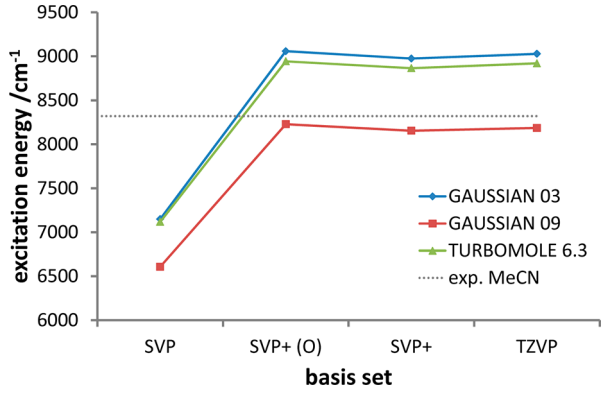


**Figure 2.** Basis set dependence of TDDFT-BLYP35 results for IV-CT excitation energies of **2**, with different programs and COSMO/CPCM solvent model implementations in MeCN, as compared to experiment.

Again, changes from SVP+(O) to SVP+ or TZVP are minor. It is thus clear that the description of negative charge on the nitro oxygen atoms is the decisive point. Given the moderate size of the systems of the present study, we opted nevertheless for use of TZVP basis sets throughout.

Efficiency considerations for larger systems may nevertheless render a mixed basis with addition of diffuse functions to selected atoms an attractive alternative. We note in passing that the Gaussian 09 CPCM implementation gives a slightly (about 500−700 cm$^{-1}$) lower excitation energy for **2**, and thus somewhat better agreement with experiment, than that in Gaussian 03 or the COSMO implementation in TURBOMOLE 6.3.

**BLYP35/TZVP Gas-Phase Results.** A number of previous computational studies have addressed the gas-phase molecular


dx.doi.org/10.1021/ct300545x | J. Chem. Theory Comput. 2012, 8, 4189−4203

Table 1. Comparison of Computed Dipole Moments ($\mu$) in debye, ET Barriers ($\Delta H^{\ddagger}$) in kJ mol$^{-1}$, C−N Bond Lengths ($d_1$, $d_2$) in Å, IV-CT Excitation Energies ($E_1$) as well as Electronic Coupling Matrix Elements ($2H_{ab}$) in cm$^{-1}$, and Transition Dipole Moments ($\mu_t$) in D[a]

| | $\mu$ | $\Delta H^{\ddagger}$ | $\Delta H^{\ddagger}$ exp.[b] | $d_1$(C−N) | $d_2$(C−N) | $E_1$ | $E_1$ exp.[b] | $2H_{ab}$[d] | $\mu_t$[e] |
|---|---|---|---|---|---|---|---|---|---|
| **1** | 0.05 | 0.0 | −[c] | 1.398 | 1.398 | 12 864 | 11 000 | 12 846 | 7.28 (7.29) |
| **2** | 11.79 | 12.5 | 12.0 | 1.387 | 1.467 | 8140 | 8320 | 3420 | 1.68 (5.72) |
| **3** | 15.09 | 18.1 | 18.4 | 1.386 | 1.462 | 8365 | 9360 | 2249 | 1.26 (7.98) |
| **4** | 0.40 | 0.0 | −[c] | 1.401 | 1.404 | 9750 | 8500 | 9742 | 9.68 (0.69) |
| **5** | 19.06 | 5.5 | 11.3 | 1.384 | 1.450 | 10 207 | 11 300 | 6640 | 9.65 (15.89) |
| **6** | 18.76 | 13.6 | 8.8 | 1.389 | 1.461 | 11 143 | 12 800 | 5435 | 3.79 (13.38) |

[a]BLYP35/TZVP/CPCM results in MeCN using Gaussian 09. Dipole moments are given relative to the center of charge. Results in DCM are provided in Table S7. [b]ESR-based ET barriers and IV-CT excitation energies from refs 33, 44, 45, 47, 51, 53, and 54. [c]Class III system. [d]Excitation energies obtained exactly at the symmetrical structure. [e]Transition dipole moments in parentheses obtained exactly at the symmetrical structure.

and electronic structures of some of the title systems, with somewhat uncertain conclusions: UHF/6-31+G* and UMP2/6-31+G* gas-phase calculations on **2** gave a localized structure and a substantial ET barrier of ca. 28 kJ mol$^{-1}$ at UHF level.[33] The UHF calculations were, however, plagued by the usual overpolarization and thus by substantial spin contamination, and therefore also the UMP2 results are doubtful. Subsequently, a number of computational studies on **2** employed CASSCF and multireference perturbation methods (MR-MP2, MCQDPT2, CASPT2),[39,41−43] as well as single-point CCSD(T)[39] and CDFT calculations,[43] with widely differing results: while CASSCF calculations lack dynamical electron correlation and provide a certainly still too large ET barrier (ca. 17 kJ mol$^{-1}$),[39,42] very shallow potential curves (obtained in single-point calculations along the ET coordinate) with multiple minima and ET barriers between ca. 4 and ca. 10 kJ mol$^{-1}$ are obtained at, for example, CASPT2, MR-MP2, or CCSD(T) levels (CDFT calculations reproduced the MR-MP2 data).[43] On the basis of some of these results, a complicated four-level scheme for ET was proposed.[43] However, given that dynamical correlation favors delocalized structures and only very moderate basis sets had been used (from 6-31G* to aug-cc-pVDZ), it is very likely that the extra minima are artifacts of the too small basis sets. They should vanish in more refined post-HF calculations. Consequently, BLYP35/TZVP gives a delocalized single-minimum class III description for **2**, and in fact for all radical anions of the present study in the gas phase (only for borderline-case **3** is a slight tendency of symmetry breaking observed, Table S6, rendering this system the one most prone to localization within the present test set). Given the generally excellent performance of the BLYP35/TZVP level in the presence of a solvent model (see below), we believe that it provides a more realistic description of the gas-phase potential energy surfaces than obtained in previous studies. 1,3-Dinitrobenzene radical anion **2** is thus very likely a delocalized class III case in the gas phase, and the same holds for the five other radical anions.

**Performance of the BLYP35/TZVP/CPCM Approach in Solution.** Our previous validation work concentrated on the BLYP-based global hybrid of eq 1, where the exact-exchange admixture $a$ had been optimized as an empirical parameter to $a$ = 0.35 (BLYP35).[36] Before going into a detailed comparison of different functionals, we thus evaluate (continuum-model) solution results for **1**−**6** obtained at the BLYP35 level (Table 1). For comparability with the larger set of functionals discussed below, we report TZVP calculations obtained with Gaussian 09 and the corresponding CPCM implementation (see Computational Details; results obtained with other codes are provided in Tables S2 and S3 in the Supporting Information). BLYP35/TZVP ground-state structure optimizations in MeCN (see Table 1, results for the less polar DCM are found in Table S7 in the Supporting Information) provide still essentially delocalized (class III) structures for **1** and **4**, as indicated by negligible structural distortions (independent of the starting point of the optimization), dipole moments, and thermal ET barriers. These results are consistent with experimental observation in the same solvent (see above).

In contrast, the optimizations for radical anions **2**, **3**, and **6** in MeCN (Table 1) give clearly localized structures with double-well potentials and ET barriers between 12 and 18 kJ mol$^{-1}$ (the optimizations with TURBOMOLE 6.3 give somewhat larger barriers in this solvent, Table S8 in the Supporting Information). These three radicals are thus characterized as class II in MeCN at this level, again consistent with experimental evidence. The computed ET barriers are in the right range (Table 1). We should also note that the ESR-based barriers come with non-negligible error bars, due to limited accuracy of the underlying Eyring plots for limited temperature ranges (barriers derived more indirectly from optical spectra differ[45,51]). Various approximations involved in the computational determination (cf., Computational Details) also limit the achievable accuracy.

The tolane-bridged radical anion **5** is closest to the class II/III borderline in our calculations in MeCN. The optimized structure is distorted, but the ET barrier is only 5.5 kJ mol$^{-1}$ in the Gaussian 09 calculations. The switch to TURBOMOLE 6.3 and its COSMO solvation model increases the barrier to 10.2 kJ mol$^{-1}$, close to the ESR-based estimate (Table S8). Obviously, fine details of the implementation (solvent model, possibly SCF, and structure optimization convergence) do already cause non-negligible changes in this borderline case. Yet, the borderline character of **5** is in line with the observation of a change to a class III situation when moving to lower-$\lambda_S$ solvents like HMPA.[55,56] Overall, we see that the BLYP35/TZVP/CPCM (or COSMO) based approach recovers very well the ground-state characteristics of these six dinitro-aromatic MV radical anions in aprotic polar solvents like MeCN, thus extending our previous validation on arylamine radical cations.

Turning to the IV-CT excitation energies in MeCN (Table 1), the performance of the BLYP35 calculations resembles again that obtained previously for MV arylamine radical cations: for the class III systems **1** and **4**, the excitation energies are overestimated by about 1800 and 1250 cm$^{-1}$, respectively, and the transition dipole moments are also overestimated. In case of the broad bands of class II systems, the experimental band

maximum is more difficult to identify. Taking the reported data, we nevertheless come to the conclusion that the BLYP35 calculations tend to underestimate these values by about 1000 $cm^{-1}$, again consistent with the previous results for MV arylamine radical cations.[36,37] Only in case of **2** is the computed value within 200 $cm^{-1}$ of the experimental band maximum. As the excitation energies computed with TURBOMOLE 6.3 (Table S8 in Supporting Information) are about 1000 $cm^{-1}$ larger than the Gaussian values, they tend to agree better with experiment, of course except for **2**. Systematic differences between the solvent models account for most of the discrepancies between the Gaussian 09 and TURBOMOLE 6.3 results.

**Evaluation of Different Density Functionals.** Despite its excellent performance above and in our previous studies,[36,37] BLYP35 is not a functional that is optimal for general main-group thermochemistry, as the exact-exchange admixture is too high for the simple form of the hybrid. It is known, however, that the inclusion of local kinetic energy density in so-called meta-GGA global hybrids allows high exact-exchange admixtures while maintaining accurate main-group thermochemistry. The smaller size of the present test systems as compared to the previous work has allowed us a systematic evaluation also of such highly parametrized meta-GGA hybrids, as implemented in Gaussian 09 (but not yet in TURBOMOLE), together with range hybrids and a double hybrid (cf., Computational Details). Given that $E_{xx}$ admixture to the functional is known to diminish self-interaction errors, the amount of exact exchange is expected to be decisive for the performance of a given functional on the question of localization/delocalization.[36] This is borne out by the present results. For global hybrids like BLYP35 ($a$ = 0.35), and for meta-GGA global hybrids like BMK ($a$ = 0.42), M05 ($a$ = 0.27), M06 ($a$ = 0.28), M05-2X ($a$ = 0.54), and M06-2X ($a$ = 0.56), parameter $a$ clearly controls the $E_{xx}$ admixture. The same holds for the double hybrid B2PLYP ($a$ = 0.53), albeit the MP2-like correlation term is expected to have a larger effect on the performance than the other correlation functionals in the comparison. The range hybrids are more difficult to compare to, as the $E_{xx}$ admixture is not a constant but depends on interelectronic distance.

Structure optimizations for the class III system **1** gave delocalized structures with negligible structural distortions, dipole moments, or ET barriers in both DCM and MeCN solvents for all meta-GGA global hybrids, the B2PLYP double hybrid, and the CAM-B3LYP range hybrid (Table S9 in the Supporting Information). Only the range hybrids LC-BLYP and $\omega$B97X provide some indications of incipient (unphysical) symmetry breaking. For $\omega$B97X, the ET barriers are negligible, however, and the values for LC-BLYP are also still small. In any case, these observations suggest already that the overall exact-exchange admixture and thus the tendency toward symmetry breaking for these two range hybrids are particularly large as compared to the other functionals in the present study. Figure 3 compares the IV-CT excitation energies for **1** with the whole set of functionals in both solvents. In agreement with our previous experience,[36,37] the dependence on exact-exchange admixture for this class III system is only moderate. This is indicated by the fact that, for example, the M05 and M06 functionals and their "double-exchange" analogues M05-2X and M06-2X all overestimate the excitation energy by similar amounts, as do BLYP35 and BMK.

Only the B2PLYP double hybrid gives a lower value (the TDDFT treatment in this case involves a CIS(D) formalism for

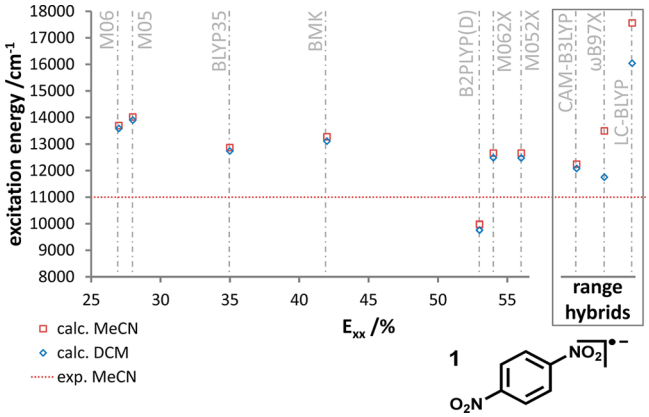


**Figure 3.** Computed excitation energies for the class III system **1** in MeCN and DCM depending on $E_{xx}$ admixture of the density functional, as compared to the experimental value in MeCN (11 000 $cm^{-1}$).[45]

the MP2 term, in contrast to the CIS-type treatment for all other functionals). Among the range hybrids, CAM-B3LYP gives a value similar to that of the global hybrids. The fact that $\omega$B97X in MeCN and LC-BLYP in both solvents give even much larger excitation energies, and thus larger deviations from experiment, is due to the incipient, erroneous ground-state symmetry breaking at these levels (see above). Transition dipole moments are overestimated systematically, increasing with $E_{xx}$ admixture (Table S9).

Table 2 summarizes some of the most relevant computed ground-state characteristics for the class II radical anion **2** (in

**Table 2. Computed Ground-State Properties ($\mu$ in debye, $\Delta H^{\ddagger}$ in kJ $mol^{-1}$, Bond Lengths $d_1$, $d_2$ in Å) with Different Functionals for 2 in MeCN[a]**

| functional/exp. | $E_{xx} = a$ | $\mu$ | $\Delta H^{\ddagger}$ | $d_1$(C–N) | $d_2$(C–N) |
|---|---|---|---|---|---|
| M06 | 0.27 | 9.99 | 1.6 | 1.391 | 1.463 |
| M05 | 0.28 | 8.25 | 0.1 | 1.407 | 1.453 |
| BLYP35 | 0.35 | 11.79 | 12.5 | 1.387 | 1.467 |
| BMK | 0.42 | 11.88 | 14.2 | 1.385 | 1.464 |
| B2PLYP | 0.53 | 12.78 | 0.9 | 1.393 | 1.475 |
| B2PLYPD | 0.53 | 12.78 | 0.9 | 1.393 | 1.476 |
| M06-2X | 0.54 | 11.97 | 23.5 | 1.388 | 1.475 |
| M05-2X | 0.56 | 12.09 | 23.1 | 1.385 | 1.469 |
| CAM-B3LYP | | 11.93 | 19.4 | 1.387 | 1.470 |
| $\omega$B97X | | 12.10 | 28.5 | 1.388 | 1.476 |
| LC-BLYP | | 12.62 | 39.9 | 1.380 | 1.464 |
| ESR[45] | | | 11.97 ± 0.29 | | |

[a]TZVP/CPCM results obtained with Gaussian 09. Dipole moments are given relative to the center of charge. Results in DCM are provided in Table S10.

MeCN). Here, the dependence on exact-exchange admixture is obvious: the M05 and M06 functionals with less than 30% exact-exchange admixture give a slight structural distortion but negligible energy lowering relative to the symmetrical transition-state structure (and thus negligible ET barriers). Here, the dipole moments are no perfect indicators of symmetry breaking, as even the symmetrical structure has a dipole moment of about 5.74 D (symmetry breaking enhances it by about 6 D). All global hybrids with $a$ > 0.3, and all three range hybrids give localized structures, albeit with quite different ET barriers. BLYP35 and BMK provide barriers

closest to the ESR-based estimate of about 12 kJ mol$^{-1}$. The M05-2X and M06-2X functionals overestimate the barrier, probably indicating somewhat too large $E_{xx}$ admixture. Among the range hybrids, CAM-B3LYP appears to perform best, falling between the BLYP35, BMK values and the M05-2X and M06-2X data, whereas the very large barriers obtained with $\omega$B97X and LC-BLYP confirm the notion of overlocalization and excessive $E_{xx}$ admixture. We note that recent TDDFT studies with $\omega$B97X came to similar conclusions.[85] Recent B3LYP/6-311++G(d,p)/PCM calculations on **2** gave structural symmetry breaking in DMSO.[35] Our own calculations at B3LYP/TZVP level confirm this. However, a negligible ET barrier of 0.7 kJ mol$^{-1}$ is found (0.6 kJ mol$^{-1}$ in MeCN).

Interestingly, the double hybrid B2PLYP also gives a structural distortion and a dipole moment for **2** close to the results of the better-performing functionals (e.g., BLYP35, cf., Figure 4, Table 2), independent of the presence or absence of a

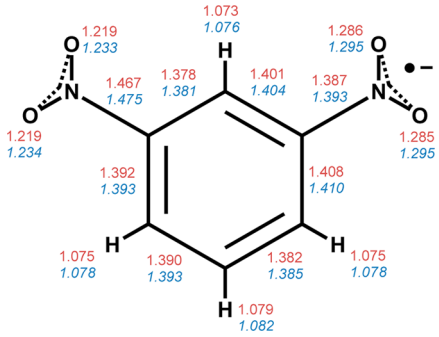


**Figure 4.** Computed ground-state bond lengths in angstroms for **2** in MeCN (CPCM) at BLYP35 (upper values, red) and B2PLYP (lower values, blue) levels.

dispersion correction. Yet the computed ET barrier is negligible, despite the relatively large exact-exchange admixture of 53%. Closer inspection reveals that in the absence of the MP2 correlation term, the ET barrier would be 32 kJ mol$^{-1}$. The MP2 term (over)stabilizes the symmetrical transition state by almost the same amount and thus creates a much too shallow double-minimum potential.

As expected for the class II system **2**, the dependence of the IV-CT excitation energy on the functional is much more pronounced than for the class III system **1** above. Figure 5 shows that M05 and M06 underestimate the energy dramatically, due to the erroneously delocalized ground-state structures. The BLYP35 and BMK functionals, with their "intermediate" $a$-values, perform best, whereas exact-exchange admixtures above 50%, as in M05-2X, M06-2X, or in the double hybrid B2PLYP, cause an overestimate on the order of 4000 cm$^{-1}$. In the latter case, we ascertained by B2PLYP TDDFT calculations at the BLYP35-optimized structure and vice versa that this is not a problem of the ground-state structure (Table S11 in the Supporting Information). Completely unrealistic excitation energies are obtained with the $\omega$B97X and LC-BLYP range hybrids, whereas CAM-B3LYP results are too high only by about 2000 cm$^{-1}$ (in MeCN).

The dependences of thermal ET barriers and IV-CT excitation energies on functional for such a class II system thus go in parallel, and the previously evaluated BLYP35 functional performs quite well for both properties (this holds also for the other class II systems). As indicated above, however, BLYP35 is not a functional optimized for general

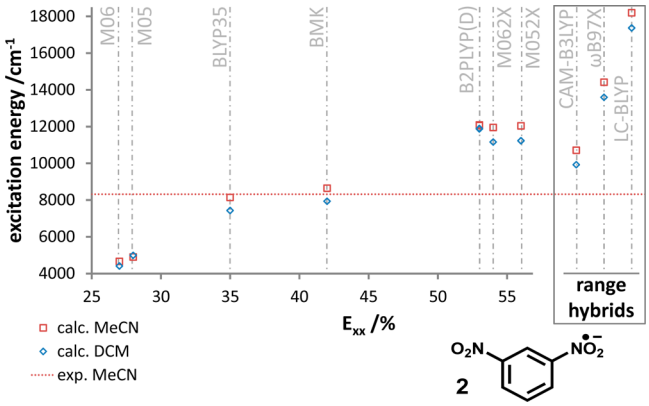


**Figure 5.** Computed excitation energies for the class II system **2** in MeCN and DCM depending on $E_{xx}$ admixture of the density functional, as compared to the experimental value in MeCN (8320 cm$^{-1}$).[33,45]

main-group thermochemistry. In contrast, the more highly parametrized meta-GGA hybrid BMK[73] is rather successful on this score, despite its 42% exact-exchange admixture, and it performs also very well for the current set of MV compounds (see also below). It may thus be an interesting alternative, albeit it is not yet available in quite as many efficient codes. A potentially interesting global hybrid functional without meta-GGA part and with similar exact-exchange admixture ($a$ = 0.428) is MPW1K,[86] which has already been used in a few cases for transition-metal MV systems.[87,88] It does indeed give very similar (slightly inferior) results for **2** as BMK: in MeCN, we obtain a class II system with an ET barrier of 16.4 kJ mol$^{-1}$ and an IV-CT excitation energy of 10 407 cm$^{-1}$ (for **1**, we find a class III structure with an excitation energy of 12 952 cm$^{-1}$). Given the similarity to the BMK results, we refrain from a more detailed discussion of MPW1K. Previous RISM-MCSCF calculations[34] for **2** are discussed further below in the context of our D-COSMO-RS results.

Given the above results for **1** and **2**, we provide now a somewhat narrower comparison of functionals for **3**–**6**, looking at global hybrids and meta-GGA global hybrids only. Table 3 shows computed ground-state parameters for **3** in MeCN. As this is the most clear-cut class II system of the six dinitroaromatic radical anions of the present test set (cf., Table 1), even the M05 and M06 functionals provide notable charge localization, albeit with insufficient asymmetry, too small

**Table 3. Computed Ground-State Properties ($\mu$ in debye, $\Delta H^{\ddagger}$ in kJ mol$^{-1}$, Bond Lengths $d_1$, $d_2$ in Å) with Different Functionals for 3 in MeCN[a]**

| functional/exp. | $E_{xx} = a$ | $\mu$ | $\Delta H^{\ddagger}$ | $d_1$(C–N) | $d_2$(C–N) |
|---|---|---|---|---|---|
| M06 | 0.27 | 13.59 | 5.5 | 1.388 | 1.465 |
| M05 | 0.28 | 13.02 | 3.7 | 1.393 | 1.474 |
| BLYP35 | 0.35 | 15.09 | 18.1 | 1.386 | 1.462 |
| BMK | 0.42 | 15.13 | 20.4 | 1.384 | 1.459 |
| M06-2X | 0.54 | 15.29 | 30.3 | 1.387 | 1.471 |
| M05-2X | 0.56 | 15.41 | 30.4 | 1.383 | 1.465 |
| ESR (MeCN)[51] | | | 18.4 ± 0.84 | | |
| ESR (DMF)[51] | | | 13.0 ± 1.25 | | |

[a]TZVP/CPCM results obtained with Gaussian 09. Dipole moments are given relative to the center of charge. Results for DCM are provided in Table S12.

ET barriers, and a lower dipole moment than expected for a localized structure (even B3LYP with $a$ = 0.20 gives already a partly localized class III situation for **3** in MeCN). As compared to the ESR-based ET barrier in MeCN, the BLYP35 and BMK functionals again perform best, whereas the M05-2X and M06-2X functionals give too large barriers at the given level of solvent model, just as found for **2** above. The experimental barrier is ca. 5 kJ mol$^{-1}$ lower in DMF than in MeCN (Table 3). This can clearly not be modeled at the continuum-solvent level, as both solvents have essentially identical dielectric constants (Table S5). We will return to this question further below. The same holds for the IV-CT excitation energy, which is about 1200 cm$^{-1}$ lower in DMF than in MeCN (Figure 6).

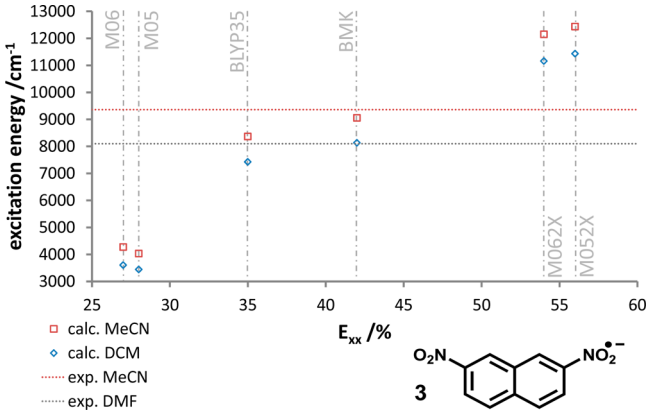


**Figure 6.** Computed excitation energies for the class II system **3** in MeCN and DCM depending on $E_{xx}$ admixture of the density functional, as compared to the experimental value in MeCN (9360 cm$^{-1}$) and in DMF (8100 cm$^{-1}$) (see refs 33 and 45).

Focusing on the MeCN computational results, we see again the typical behavior we found for class II systems (cf., Figure 6 and refs 36, 37), that is, a strong dependence on exact-exchange admixture and best performance for BLYP35 and BMK. Measured transition dipole moments $\mu_t$ are 1.04−1.12 D, depending on the method of determination.[33] They are reasonably well reproduced by BLYP35, BMK, M05-2X, and M06-2X but overestimated by the M05 and M06 functionals (cf., Table S12 in the Supporting Information).

To our knowledge, radical anion **3** is the first MV system for which ground-state structure optimizations including a solvation model had been carried out. Nelsen, Clark, and co-workers used a semiempirical AM1 Hamiltonian with subsequent single-excitation configuration interaction within an active orbital space of 70 MOs, AM1-CIS(70), together with COSMO solvation for a variety of dielectric constants $\varepsilon$.[33] To connect to the present work, we can look at their results for MeCN: charge localization has been obtained, with structural distortion similar to that in our BLYP35/TZVP results (somewhat more for the reduced side, less for the neutral side), and an ET barrier of about 30 kJ mol$^{-1}$ (i.e., too large, best comparable to the M05-2X or M06-2X results, cf., Table 3). The computed IV-CT excitation energy of ca. 8950 cm$^{-1}$ is also close to our BLYP35 or BMK data (cf., Figure 6). Given the semiempirical basis of the approach, this is an excellent performance. So far it remains unclear, however, whether it could be generalized straightforwardly to other systems (e.g., regarding the active orbital space).

Results with different functionals for the class III system **4** are very similar to those for **1** above and are provided in the Supporting Information (Table S13 and Figure S1). The only difference observed is that the M05-2X and M06-2X functionals induce first indications of symmetry breaking in MeCN and DCM (with very small ET barriers but strong effects on the IV-CT excitation energies). All other functionals provide clearly delocalized, symmetrical structures.

As discussed above, the tolane-bridged **5** is closest to the class II/III transition in aprotic solvents. It goes from being delocalized in less polar solvents like HMPA or THF to being localized in DCM or MeCN. Table 4 shows that with none of the functionals, the continuum-solvent model-based protocol can reproduce this transition: the M05 or M06 functionals with $a$ < 0.3 give a delocalized structure in THF, DCM, and MeCN, whereas the other four functionals in the list give localized structures in all three solvents.

In this case, the larger ET barriers obtained with the M05-2X and M06-2X functionals appear to be closer to the ESR-derived values in DCM and MeCN than the BLYP35 or BMK results. This contrasts to all other class II cases in this study, where the M05-2X and M06-2X barriers are too high. The fact that a continuum solvent model reaches its limits here becomes obvious when comparing THF and DCM: both have very similar dielectric constants (Table S5). Yet the system is experimentally on the class III side in the former and on the class II side in the latter. This clearly calls for improved treatments of solvent effects beyond the continuum solvent level (see below).

**Table 4. Computed Ground-State Properties ($\mu$ in debye, $\Delta H^{\ddagger}$ in kJ mol$^{-1}$) with Different Functionals for 5 in MeCN, DCM, and THF[a]**

| | | MeCN | | DCM | | THF | |
|---|---|---|---|---|---|---|---|
| functional/exp. | $E_{xx}$ = $a$ | $\mu$ | $\Delta H^{\ddagger}$ | $\mu$ | $\Delta H^{\ddagger}$ | $\mu$ | $\Delta H^{\ddagger}$ |
| M06 | 0.27 | 0.01 | 0.0 | 0.13 | 0.0 | 0.04 | 0.1 |
| M05 | 0.28 | 0.44 | 0.0 | 0.25 | 0.0 | 0.02 | 0.0 |
| BLYP35 | 0.35 | 19.06 | 5.5 | 16.10 | 2.4 | 15.21 | 1.9 |
| BMK | 0.42 | 19.29 | 6.3 | 16.69 | 3.1 | 15.81 | 0.1 |
| M06-2X | 0.54 | 21.60 | 14.4 | 20.03 | 9.9 | 19.55 | 0.1 |
| M05-2X | 0.56 | 21.74 | 15.5 | 20.24 | 10.9 | 19.79 | 0.0 |
| ESR (MeCN)[51] | | | 11.3 ± 1.7 | | | | |
| ESR (DMF)[51] | | | 13.8 ± 1.88 | | | | |
| ESR (DCM)[51] | | | | | 11.5 ± 0.88 | | –[b] |

[a]TZVP/CPCM results obtained with Gaussian 09. Dipole moments are given relative to the center of charge. Further results in DCM are provided in Table S14. [b]Class III system.

IV-CT excitation energies in MeCN or DCM (Figure 7) are dramatically underestimated at M05 or M06 levels, mainly due

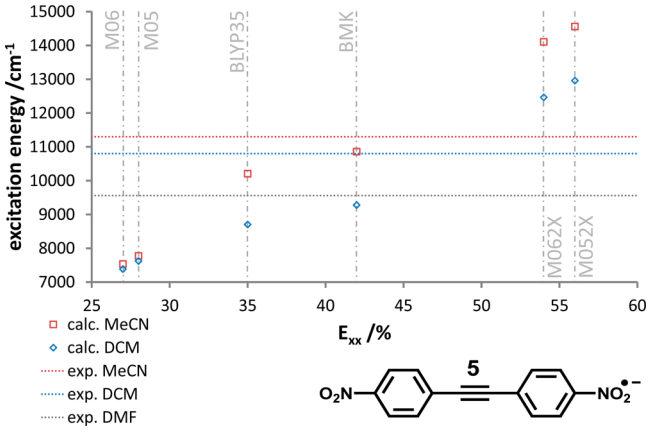


**Figure 7.** Computed excitation energies for **5** in MeCN and DMF depending on $E_{xx}$ admixture of the density functional, as compared to the experimental values 11 300 $cm^{-1}$ (MeCN), 10 800 $cm^{-1}$ (DCM), and 9560 $cm^{-1}$ (DMF) (see ref 53).

to the erroneously delocalized structures. The dependence of these energies on $\varepsilon$ is significant for the other functionals. Looking at the MeCN results, agreement with experiment is again most favorable for the BLYP35 and BMK functionals, as for other class II systems, whereas M05-2X and M06-2X overestimate the values by about 3000 $cm^{-1}$ (Figure 7). Computed transition dipole moments are generally overestimated, in particular for the M05 and M06 functionals, probably again due to the delocalized ground-state structures. IV-CT excitation energies in THF (5860 $cm^{-1}$) are generally overestimated dramatically (Table S14 in the Supporting Information, which gives also further TDDFT data for several experimentally available excitations). While an overestimate for class III systems is typical, part of the errors arises from erroneous ground-state symmetry breaking for functionals with $a > 0.3$. Clearly, the solvent description for THF is not realistic, possibly in part due to the ability of THF to coordinate to the counter-cations (see below for D-COSMO-RS calculations).

Resonance Raman measurements on **5** by Telo, Nelsen, and co-workers[54] show a shift of the C≡C stretching frequency to lower values when going from localized to delocalized ground-state structures by choice of the solvent. In MeCN, two peaks have been observed and were assigned to a localized (2166 $cm^{-1}$) and a delocalized species (2146 $cm^{-1}$), while only the latter remains and is shifted to lower values in THF. This shift is reproduced at BLYP35/TZVP/CPCM level (Table 5), even though the (unscaled) frequencies are about 100 $cm^{-1}$ too high in absolute terms (a scaling factor of 0.95 brings computed frequencies close to experiment). The difference between

**Table 5. Calculated Harmonic C≡C Stretching Frequencies (in $cm^{-1}$) for 5[a]**

| solvent | localized[b] | delocalized[c] |
|---|---|---|
| MeCN | 2274.6 | 2254.7 |
| DCM | 2262.5 | 2253.3 |
| THF | 2260.3 | 2253.4 |

[a]BLYP35/TZVP/CPCM results. [b]$C_1$ minimum structure. [c]Symmetrical transition-state structure.

frequencies for localized and delocalized systems diminishes with decreasing polarity of the solvent, as expected.

The dependence of the ground-state properties and IV-CT excitation energies on the functional for **6** is in line with the other, relatively clear-cut class II cases **2** and **3** (see above). The data are provided in Table S15 and Figure S2 in the Supporting Information. We only note here that BLYP35 and BMK again perform best for ET barriers and IV-CT excitation energies, and that the difference of about 5 kJ $mol^{-1}$ between the ET barriers in MeCN and DMF can of course not be modeled at the continuum solvent level, due to the almost identical dielectric constants of the two solvents. Another potential complication for **6** is the twisting between the two phenyl rings of the bridge. The relatively shallow potential energy surface for this twisting motion has to be kept in mind when judging the achievable accuracy, in particular for the IV-CT transition dipole moments (Table S15).

Let us summarize the evaluation of functionals: we have seen that the exact-exchange admixture of global hybrids influences the performance decisively. The BLYP35 ($a = 0.35$) and BMK ($a = 0.42$) functionals performed best for both class II and class III systems, including ET barriers for the former and IV-CT excitation energies for both. The BMK functional has the advantage of being optimized also for general main-group thermochemistry, but it is not yet available in many efficient codes. The MPW1K global hybrid ($a = 0.428$) may also be an option, it appears to perform similarly as BMK. Lower exact-exchange admixtures tend to overestimate delocalization, higher ones localization, with corresponding consequences for the barriers and IV-CT excitations. In terms of structural symmetry breaking for the class II case **2**, performance of the double hybrid B2PLYP resembled that of global hybrids with high exact-exchange admixture such as M06-2X. Yet the computed ET barrier was far too low, apparently due to an over-stabilization of the symmetrical transition state by the MP2 correlation term included in the functional. Among the range hybrids studied, CAM-B3LYP performed well albeit somewhat inferior to the best global hybrids (BLYP35, BMK). The ωB97X and LC-BLYP range hybrids were strongly on the overlocalized side, indicating too high exact-exchange admixture. They provided neither good ground-state properties and ET barriers nor realistic IV-CT excitation energies. In general, double hybrids and range hybrids did not offer any advantages over global hybrids for the systems and properties studied. Local hybrid functionals, with position-dependent exact-exchange admixture, appear to be a particularly promising alternative for future studies,[89−91] in particular for MV transition-metal complexes. System **5**, which is closest to the class II/III transition, exposed clearly the limitations of the continuum solvent models used in the current protocol, providing one of the motivations for turning now to the D-COSMO-RS approach.

**Direct COSMO-RS Calculations.** Above we have encountered a number of cases where continuum solvent models are beyond their limits. A continuum solvent model is characterized only by its dielectric constant $\varepsilon$, and obviously this does not include all necessary information about solvation in the present context. Specific solvation interactions enter the ET processes via outer or solvent reorganization energies, $\lambda_O$ or $\lambda_S$. The most clear-cut case where a continuum solvent model thus fails to describe matters accurately is hydrogen bonding. Yet we have also seen that the lower reorganization energy of THF versus DCM (or of HMPA vs MeCN) may favor a class III situation,

Table 6. Comparison of COSMO and D-COSMO-RS Results for Ground-State Properties ($\mu$ in debye, $\Delta H^{\ddagger}$ in kJ mol$^{-1}$, Bond Lengths $d_1$, $d_2$ in Å) and IV-CT Excitation Energies ($E_1$ in cm$^{-1}$) of 1 in Methanol, *n*-Octanol, and MeCN[a]

| solvent | solvent model | $\mu$ | $\Delta H^{\ddagger b}$ | $d_1$(C−N) | $d_2$(C−N) | $E_1$ |
|---|---|---|---|---|---|---|
| *n*-octanol | COSMO | 0.26 | 0.0 | 1.396 | 1.398 | 13069 |
| | D-COSMO-RS | 8.95 | 6.6 | 1.383 | 1.437 | 16709 |
| MeOH | COSMO | 0.31 | 0.0 | 1.395 | 1.397 | 13007 |
| | D-COSMO-RS | 9.65 | 8.2 | 1.384 | 1.440 | 17343 |
| MeCN | COSMO | 0.47 | 0.0 | 1.394 | 1.398 | 13008 |
| | D-COSMO-RS | 0.08 | 0.0 | 1.397 | 1.398 | 13097 |

[a]BLYP35/TZVP results with TURBOMOLE 6.3; more detailed results are in Table S16. Dipole moments are given relative to the center of charge. [b]The ESR-based experimental free-energy ET barrier ($\Delta G^{\ddagger}$) is 36 ± 3 kJ mol$^{-1}$ in *n*-octanol and 26 ± 2 kJ mol$^{-1}$ in MeOH.[47]

Table 7. Comparison of COSMO and D-COSMO-RS Results for Ground-State Properties ($\mu$ in debye, $\Delta H^{\ddagger}$ in kJ mol$^{-1}$, Bond Lengths $d_1$, $d_2$ in Å) and IV-CT Excitation Energies ($E_1$ in cm$^{-1}$) of 2 and 3 in MeOH and MeCN[a]

| molecule | solvent | solvent model | $\mu$ | $\Delta H^{\ddagger}$ | $d_1$(C−N) | $d_2$(C−N) | $E_1$ |
|---|---|---|---|---|---|---|---|
| **2** | MeOH | COSMO | 12.53 | 17.6 | 1.388 | 1.466 | 9214 |
| | | D-COSMO-RS | 14.86 | 43.1 | 1.393 | 1.469 | 14 807 |
| | | exp. | | 43.1[b] | | | |
| | MeCN | COSMO | 12.56 | 17.8 | 1.388 | 1.466 | 9267 |
| | | D-COSMO-RS | 11.79 | 12.8 | 1.387 | 1.467 | 7989 |
| | | exp. | | 11.97 ± 0.29[c] | | | 8320[d] |
| **3** | MeOH | COSMO | 15.91 | 23.0 | 1.387 | 1.461 | 9522 |
| | | D-COSMO-RS | 18.75 | 48.2 | 1.390 | 1.463 | 15 088 |
| | | exp. | | 49.1[b] | | | |
| | MeCN | COSMO | 15.95 | 23.2 | 1.387 | 1.461 | 9591 |
| | | D-COSMO-RS | 15.06 | 18.4 | 1.386 | 1.462 | 8219 |
| | | exp. | | 18.4 ± 0.84[c] | | | 9360[d] |

[a]BLYP35/TZVP results with TURBOMOLE 6.3; more detailed results in Tables S17 and S18. Dipole moments are given relative to the center of charge. [b]ESR-based experimental free-energy ET barriers ($\Delta G^{\ddagger}$).[52] [c]ESR-based $\Delta H^{\ddagger}$ value.[51] [d]IV-CT excitation energies from ref 33.

despite the similar $\varepsilon$-values. Similar considerations hold for DMF (or HMPA) versus MeCN. It is, however, possible that the good cation coordination properties[92] of THF or HMPA play a decisive role, and this remains beyond the scope of the present study.

A more realistic microscopic treatment of solvation based on explicit ab initio molecular dynamics (MD) simulations, typically with periodic boundary conditions, is in principle possible for the present, moderately sized test systems and will be pursued elsewhere. However, the computational and manpower effort involved in such studies is on a scale entirely different from that of the protocol discussed so far. Such methods are currently not easily generalized to routine work on a large number of extended systems of chemical interest. A computational scheme covering the middle ground between continuum solvent models and full ab initio MD is thus highly desirable. In the context of ET parameters and MV systems, we are aware of one study on **2** using the RISM-MCSCF approach,[34] which combines CASSCF calculations on the solute with a molecular-mechanics/Monte Carlo/statistical thermodynamics treatment of the solvent (MeCN and MeOH were compared). Because of the shortcomings of the ROHF and CASSCF wave functions used (see also above), the computed ET barriers in that work were significantly overestimated, by about a factor 2−3. Yet, the increase in going from aprotic MeCN to the protic MeOH was at least qualitatively reproduced.[34]

Together with the BLYP35/TZVP level for treating the electronic structure, we will now evaluate for some examples out of the test set **1**−**6** the D-COSMO-RS method (see the Computational Details).[61,81,93−95] While **1** is a delocalized class III system in aprotic solvents, it localizes in alcoholic solvents. Given that alcohols have dielectric constants in a range similar to that of aprotic solvents (cf., Table S5), it is not to be expected that this can be simulated with continuum solvent models. Indeed, at the BLYP35/TZVP/COSMO level, **1** remains delocalized in both methanol and *n*-octanol (Table 6). When switching to the D-COSMO-RS level, this changes fundamentally: now **1** becomes a localized class II system in alcoholic solution, as indicated by the structural distortions, the dipole moment, and the computed ET barrier, which amounts to somewhat less than one-half of the ESR-based values (Table 6). The computed IV-CT excitation energy is also increased dramatically as compared to the COSMO result, as expected for the formation of a double-well potential (see Figure 1, Table 6; no spectra in alcohols are available so far). That is, the corrections that the D-COSMO-RS approach makes to an idealized conductor-like screening do indeed allow a modeling of the transition to class II character in protic solvents. The somewhat too small barrier might suggest a certain underestimate of the specific solvation effects, but we reserve judgment until the evaluation of more data below. The control experiment is to compare COSMO and D-COSMO-RS results also in an aprotic solvent like MeCN. Here, the differences between the two approaches are much smaller, and the system remains a class III case even upon inclusion of the RS correction terms (Table 6). We note in passing that ion pairing effects are expected to be much less important in polar, protic solvents than they are in low-polarity solvents (or in the solid state),[46] and they can be excluded as the origin of the charge localization (cf., section 2).

Table 8. Comparison of COSMO and D-COSMO-RS Results for Ground-State Properties ($\mu$ in debye, $\Delta H^{\ddagger}$ in kJ mol$^{-1}$, Bond Lengths $d_1$, $d_2$ in Å) and IV-CT Excitation Energies ($E_1$ in cm$^{-1}$) of 5 in THF and DCM[a]

| solvent | solvent model | $\mu$ | $\Delta H^{\ddagger}$ | $d_1$(C−N) | $d_2$(C−N) | $E_1$ |
|---|---|---|---|---|---|---|
| THF | COSMO | 16.08 | 2.87 | 1.385 | 1.443 | 8955 |
| | D-COSMO-RS | 13.22 | 1.61 | 1.389 | 1.439 | 8318 |
| | exp. | | –[b] | | | 5860[d] |
| DCM | COSMO | 17.35 | 4.04 | 1.384 | 1.445 | 9428 |
| | D-COSMO-RS | 18.39 | 5.32 | 1.383 | 1.446 | 9784 |
| | exp. | | 11.50 ± 0.88[c] | | | 10 800[e] |

[a]BLYP35/TZVP results with TURBOMOLE 6.3; more detailed results in Table S20. Dipole moments are given relative to the center of charge. [b]Class III in THF. [c]ESR-based value.[51] [d]Reference 53. [e]Reference 51.

Table 9. Comparison of COSMO and D-COSMO-RS IV-CT Excitation Energies (in cm$^{-1}$) in Different Solvents for 1−4[a]

| | solvent model | DCM | MeCN | DMF | exp. (MeCN) | exp. (DMF) |
|---|---|---|---|---|---|---|
| **1** | COSMO | 13 074 | 13 008 | 13 008 | 11 000[b] | 10 820[c] |
| | D-COSMO-RS | 13 000 | 13 097 | 13 142 | | |
| **2** | COSMO | 8049 | 9267 | 9268 | 8320[c] | |
| | D-COSMO-RS | 8471 | 7989 | 7535 | | |
| **3** | COSMO | 8012 | 9591 | 9592 | 9360[d] | 8100[d] |
| | D-COSMO-RS | 8433 | 8219 | 7763 | | |
| **4** | COSMO | 10 134 | 11 188 | 11 189 | | 8500[c] |
| | D-COSMO-RS | 10 255 | 10 227 | 10 170 | | |

[a]BLYP35/TZVP results with TURBOMOLE 6.3; more detailed results in Tables S16−S19. [b]Reference 45. [c]Reference 44. [d]Reference 33.

ESR studies in alcoholic solvents are also available for **2** and **3**. As both radical anions are already localized in aprotic solvents, here the effect of hydrogen bonding must be quantitative rather than qualitative. Indeed, for both radicals, the measured ET barriers in alcohols are about twice as large as those in MeCN. Table 7 compares the COSMO and D-COSMO-RS results for both systems in MeOH and MeCN. The effect of the RS correction terms for the acetonitrile results is small, as expected. The slightly reduced ET barriers agree better with experiment. In contrast, for MeOH, a striking increase of the ET barrier is observed as compared to the COSMO data. Indeed, the RS corrections bring the computed values remarkably close to the ESR-based estimates for both radical anions. The extra deepening of the double-well potential due to hydrogen bonding is reflected in more pronounced asymmetry of the minimum structure and a somewhat increased dipole moment in MeOH versus MeCN (D-COSMO-RS results in Table 7).

The IV-CT excitation energies are also increased substantially in both cases. As no UV/vis data in alcohols are available so far for any of these systems, the magnitude of this increase is a pure prediction for which experimental verification will be interesting to see. The strikingly good agreement of the ET barriers with experiment for **2** and **3** in alcohols does not support the above presumption based on the results for **1**, that the hydrogen-bonding effects may be underestimated by the D-COSMO-RS approach. The results of the only previous application of D-COSMO-RS, to *g*-tensors of nitroxide radicals,[38] suggest that the effects of hydrogen bonding may have been underestimated somewhat. More work on a diverse set of questions will be needed to evaluate in detail the quantitative accuracy of the model.

Less spectacular effects of specific solvation are expected for aprotic solvents. Nevertheless, we have seen above that, for example, the transition of **5** from a class III situation in THF to a class II situation in DCM also cannot be described by a continuum solvent model, given the very similar dielectric constants (cf. Table S5). Indeed, the COSMO results are almost equal for THF and DCM (Table 8). The RS corrections reduce ET barrier and IV-CT excitation energy somewhat for THF and increase both somewhat for DCM. While these corrections go into the right direction, the qualitative change from a class III system in THF to a class II system in DCM is insufficiently reproduced. For both solvents, extremely shallow double-well potentials are obtained, consistent with the borderline character of **5**. The D-COSMO-RS ET barrier in DCM is >5 kJ mol$^{-1}$, about one-half the ESR-based estimate, whereas the value in THF is below 2 kJ mol$^{-1}$. Because of the remaining structural distortion, the IV-CT excitation in THF is overestimated substantially. One aspect that may be important but cannot be modeled by either COSMO or D-COSMO-RS levels is the better cation coordination ability of THF versus DCM, which may remove some residual ion pairing.

Finally, we also saw above substantial quantitative differences of the IV-CT excitation energies in MeCN and DMF for class II systems, despite the very similar dielectric constants of the two solvents. The performance of COSMO versus D-COSMO-RS for **2** and **3** in MeCN and DMF is evaluated in Table 9. As a control, the table provides also results for **1** and **4** in the same solvents. As the latter two radical anions remain class III in both aprotic solvents, a negligible solvent dependence is expected in these cases. This is indeed observed computationally: COSMO provides no, and D-COSMO-RS only small differences between the excitation energies in MeCN and DMF for **1** and **4**. COSMO also allows no distinction between the two solvents for **2** and **3**. Experimentally, values in both solvents are available for **3**. The band is blue-shifted by about 1260 cm$^{-1}$ in MeCN. The difference at D-COSMO-RS level is ca. 500 cm$^{-1}$. While this underestimates the experimental solvent shift, at least the approach distinguishes qualitatively between the two solvents, while a continuum solvent model does not. In absolute terms, D-COSMO-RS improves the agreement with experimental excitation energies for **2** in MeCN and for **3** in DMF, whereas the agreement is actually worsened for **3** in

MeCN. This comparison of absolute excitation energies involves of course also the other possible error sources of the computational approach (e.g., functional, general quality of the underlying COSMO implementation, nonequilibrium solvation, neglect of counterion effects).

Table S22 in the Supporting Information reports a similar comparison between COSMO and D-COSMO-RS results for the IV-CT excitation energies in MeCN versus DMF of **5** and **6**. Experimentally, the MeCN results are by 1740 and 1800 $cm^{-1}$, respectively, higher than the DMF data. Again, COSMO gives identical values in both solvents. Here, D-COSMO-RS provides a significantly too small correction, giving differences of ca. 240 and ca. 440 $cm^{-1}$, respectively. As for **3**, this suggests that differences in the solvent reorganization energies upon charge transfer in MeCN versus DMF are underestimated by the current D-COSMO-RS treatment. Solvent effects on ion pairing or possible solvent dynamical effects are of course again not included in the calculations.

The influence of the D-COSMO-RS corrections on the ET barriers of the class II systems in aprotic solvents amounts typically only to a few kJ $mol^{-1}$ (cf., Tables S17, S18, S20, and S21 in the Supporting Information). Regarding the differences between MeCN and DMF, no clear-cut improvement is observed relative to the experimental values. Absolute agreement with experimental barriers is also not affected in a systematic way. The differences are obviously too small. Other error sources, both on the experimental side (ESR) and on the computational side, are of similar magnitude.

## CONCLUSIONS

The current quantum-chemical approach, based on suitably chosen hybrid density functionals and either continuum solvent models or the D-COSMO-RS *ansatz*, provides the first available methodological framework that allows an essentially quantitative description of the ground-state properties and of the corresponding thermal and optical electron-transfer parameters of many organic mixed-valence compounds, from previously studied arylamine-based radical cations to the present dinitroaryl radical anions. ET barriers obtained by ESR are reproduced to a remarkable degree, and the Robin/Day classification in solution can be performed computationally with high predictive quality. IV-CT excitation energies and oscillator strengths are obtained from TDDFT calculations. The extreme importance of the solvent environment for the class II/III character of mixed-valence systems has again been demonstrated computationally. Given the success of the computational protocol for properties in solution, previous assumptions on the gas-phase electronic structure of 1,3-dinitrobenzene radical anion **2** have to be revised.

The key features of any successful approach in this field are (i) a reasonable balance between inclusion of dynamical and nondynamical electron correlation and minimal self-interaction errors and (ii) an appropriate modeling of environmental effects. On both aspects improvements are still possible: further improved generations of density functionals or accurate post-Hartree−Fock approaches may be envisioned. Even more importantly, still more sophisticated treatments of solvent effects are feasible. For example, in viscous solvents, explicit solvent dynamics during electron transfer may be important close to the class II/III borderline, and ion-pairing as well as coordination of counterions by solvent molecules may also be relevant. However, full ab initio MD simulations with subsequent thermochemical averaging, which could account for such effects, remain costly. The D-COSMO-RS approach described in this work offers a computationally expedient and useful tool. It allows us to go beyond continuum solvent models at little extra cost and has shown its great potential when dealing with protic solvent environments. Many further applications of D-COSMO-RS in different fields may be envisioned. Given the success of the present computational protocol for organic mixed-valence systems, we have now started to evaluate its performance also for the equally important and even larger field of mixed-valence transition-metal complexes. We ultimately aim at generally applicable, accurate quantum-chemical treatments of electron-transfer processes in solution.

## ASSOCIATED CONTENT

### Supporting Information

Comparison of the different program versions, basis set effects, further tabulated BLYP35/TZVP results with different program versions, detailed comparison of different functionals, further D-COSMO-RS results, and preliminary optimizations with explicit counterions. This material is available free of charge via the Internet at http://pubs.acs.org.

## AUTHOR INFORMATION

### Corresponding Author

*E-mail: martin.kaupp@tu-berlin.de.

### Notes

The authors declare no competing financial interest.

## ACKNOWLEDGMENTS

This work has been supported by the Deutsche Forschungsgemeinschaft within the Graduiertenkolleg 1221 "Control of electronic properties of $\pi$-conjugated molecules". M.R. is grateful to "Bayerisches Eliteförderungsgesetz" for a Ph.D. scholarship. We thank Christoph Lambert (Würzburg) for helpful discussions on electron-transfer theory, João P. Telo (Lisboa) for suggesting the MV dinitroaryl radical anions as interesting targets, and Günter Grampp (Graz) for some useful references.

## REFERENCES

(1) *Mixed-Valence Compounds*; Brown, D. B., Ed.; D. Reidel: Dordrecht, 1980.
(2) Launay, J.-P. *Chem. Soc. Rev.* **2001**, *30*, 386−397.
(3) Demadis, K. D.; Hartshorn, C. M.; Meyer, T. J. *Chem. Rev.* **2001**, *101*, 2655−2685.
(4) Low, P. J. *Dalton Trans.* **2005**, 2821−2824.
(5) Hankache, J.; Wenger, O. S. *Chem. Rev.* **2011**, *111*, 5138−5178.
(6) Heckmann, A.; Lambert, C. *Angew. Chem., Int. Ed.* **2012**, *51*, 326−392.
(7) Maki, A. H.; Geske, D. H. *J. Chem. Phys.* **1960**, *33*, 825−832.
(8) Ward, R. L. *J. Chem. Phys.* **1960**, *32*, 410−416.
(9) Ward, R. L. *J. Am. Chem. Soc.* **1961**, *83*, 1296−1300.
(10) Freed, J. H.; Fraenkel, G. K.; Rieger, P. H. *J. Chem. Phys.* **1962**, *37*, 1881−1882.
(11) Gendell, J.; Fraenkel, G. K.; Freed, J. H. *J. Chem. Phys.* **1962**, *37*, 2832−2841.
(12) Harriman, J. E.; Maki, A. H. *J. Chem. Phys.* **1963**, *39*, 778−786.
(13) Freed, J. H.; Fraenkel, G. K. *J. Chem. Phys.* **1963**, *39*, 326−348.
(14) Rieger, P. H.; Fraenkel, G. K. *J. Chem. Phys.* **1963**, *39*, 609−629.
(15) Freed, J. H.; Fraenkel, G. K. *J. Chem. Phys.* **1964**, *40*, 1815−1829.
(16) Freed, J. H.; Fraenkel, G. K. *J. Chem. Phys.* **1964**, *41*, 699−716.

(17) Griffith, W.; Gutch, C. J. W.; Longster, G. F.; Myatt, J.; Todd, P. F. *J. Chem. Soc. B* **1968**, 785−789.
(18) Gutch, C. J. W.; Waters, W. A.; Symons, M. C. R. *J. Chem. Soc. B* **1970**, 1261−1267.
(19) Robin, M. B.; Day, P. *Adv. Inorg. Radiochem.* **1967**, *10*, 247−422.
(20) Lambert, C.; Nöll, G. *J. Am. Chem. Soc.* **1999**, *121*, 8434−8442.
(21) Nelsen, S. F. *Chem.-Eur. J.* **2000**, *6*, 581−588.
(22) Coropceanu, V.; Malagoli, M.; André, J. M.; Brédas, J.-L. *J. Am. Chem. Soc.* **2002**, *124*, 10519−10530.
(23) Creutz, C.; Newton, M. D.; Sutin, N. *J. Photochem. Photobiol., A* **1994**, *82*, 47−59.
(24) Cave, R. J.; Newton, M. D. *Chem. Phys. Lett.* **1996**, *249*, 15−19.
(25) Cave, R. J.; Newton, M. D. *J. Chem. Phys.* **1997**, *106*, 9213−9226.
(26) Newton, M. D. *Adv. Chem. Phys.* **1999**, *106*, 303−375.
(27) Kattnig, D. R.; Mladenova, B.; Grampp, G.; Kaiser, C.; Heckmann, A.; Lambert, C. *J. Phys. Chem. C* **2009**, *113*, 2983−2995.
(28) Dehareng, D.; Dive, G.; Moradpour, A. *Int. J. Quantum Chem.* **2000**, *76*, 552−573.
(29) Fernandez, E.; Blancafort, L.; Olivucci, M.; Robb, M. A. *J. Am. Chem. Soc.* **2000**, *122*, 7528−7533.
(30) Helal, W.; Evangelisti, S.; Leininger, T.; Maynau, D. *J. Comput. Chem.* **2009**, *30*, 83−92.
(31) Coropceanu, V.; Malagoli, M.; André, J. M.; Brédas, J.-L. *J. Chem. Phys.* **2001**, *115*, 10409−10416.
(32) Kaduk, B.; Kowalczyk, T.; Van Voorhis, T. *Chem. Rev.* **2012**, *112*, 321−370.
(33) Nelsen, S. F.; Weaver, M. N.; Konradsson, A. E.; Telo, J. P.; Clark, T. *J. Am. Chem. Soc.* **2004**, *126*, 15431−15438.
(34) Yoshida, N.; Ishida, T.; Hirata, F. *J. Phys. Chem. B* **2008**, *112*, 433−440.
(35) Syroeshkin, M. A.; Mikhailov, M. N.; Mendkovich, A. S.; Rusakov, A. I. *Russ. Chem. Bull.* **2009**, *58*, 41−46.
(36) Renz, M.; Theilacker, K.; Lambert, C.; Kaupp, M. *J. Am. Chem. Soc.* **2009**, *131*, 16292−16302.
(37) Kaupp, M.; Renz, M.; Parthey, M.; Stolte, M.; Würthner, F.; Lambert, C. *Phys. Chem. Chem. Phys.* **2011**, *13*, 16973−16986.
(38) Sinnecker, S.; Rajendran, A.; Klamt, A.; Diedenhofen, M.; Neese, F. *J. Phys. Chem. A* **2006**, *110*, 2235−2245.
(39) Kayanuma, M.; Hosoi, H.; Furuya, A.; Masuda, Y.; Takano, K. *Chem. Phys. Lett.* **2010**, *494*, 139−143.
(40) Zubatyuk, R. I.; Gorb, L.; Shishkin, O. V.; Qasim, M.; Leszczynski, J. *J. Comput. Chem.* **2010**, *31*, 144−150.
(41) Mikhailov, M. N.; Mendkovich, A. S.; Kuminsky, M. B.; Kapranov, V. A.; Rusakov, A. I. *Russ. Chem. Bull.* **2005**, *54*, 2735−2737.
(42) Mikhailov, M. N.; Mendkovich, A. S.; Kuminsky, M. B.; Rusakov, A. I. *J. Mol. Struct. (THEOCHEM)* **2007**, *847*, 103−106.
(43) Ogawa, T.; Sumita, M.; Shimodo, Y.; Morihashi, K. *Chem. Phys. Lett.* **2011**, *511*, 219−223.
(44) Nelsen, S. F.; Konradsson, A. E.; Weaver, M. N.; Telo, J. P. *J. Am. Chem. Soc.* **2003**, *125*, 12493−12501.
(45) Telo, J. P.; Jalilov, A. S.; Nelsen, S. F. *J. Phys. Chem. A* **2011**, *115*, 3016−3021.
(46) Lü, J. M.; Rosokha, S. V.; Lindeman, S. V.; Neretin, I. S.; Kochi, J. K. *J. Am. Chem. Soc.* **2005**, *127*, 1797−1809.
(47) Telo, J. P.; Grampp, G.; Shohoji, M. *Phys. Chem. Chem. Phys.* **1999**, *1*, 99−104.
(48) Hosoi, H.; Masuda, Y. *J. Mol. Liq.* **2001**, *90*, 279−286.
(49) Grampp, G.; Shohoji, M.; Herold, B. J. *Ber. Bunsen-Ges. Phys. Chem.* **1989**, *93*, 580−585.
(50) Grampp, G.; Shohoji, M.; Herold, B. J.; Steenken, S. *Ber. Bunsen-Ges. Phys. Chem.* **1990**, *94*, 1507−1511.
(51) Telo, J. P.; Nelsen, S. F.; Zhao, Y. *J. Phys. Chem. A* **2009**, *113*, 7730−7736.
(52) Telo, J. P.; Shohoji, M.; Herold, B. J.; Grampp, G. *J. Chem. Soc., Faraday Trans.* **1992**, *88*, 47−51.
(53) Nelsen, S. F.; Weaver, M. N.; Telo, J. P. *J. Am. Chem. Soc.* **2007**, *129*, 7036−7043.
(54) Hoekstra, R. M.; Telo, J. P.; Wu, Q.; Stephenson, R. M.; Nelsen, S. F.; Zink, J. I. *J. Am. Chem. Soc.* **2010**, *132*, 8825−8827.
(55) Rak, S. F.; Miller, L. L. *J. Am. Chem. Soc.* **1992**, *114*, 1388−1394.
(56) Telo, J. P.; Moneo, A.; Carvalho, M.; Nelsen, S. F. *J. Phys. Chem. A* **2011**, *115*, 10738−10743.
(57) Ahlrichs, R.; Bär, M.; Häser, M.; Horn, H.; Köhmel, C. *Chem. Phys. Lett.* **1989**, *162*, 165−169.
(58) Frisch, M. J.; Trucks, G. W.; Schlegel, H. B.; Scuseria, G. E.; Robb, M. A.; Cheeseman, J. R.; Montgomery, J. A., Jr.; Vreven, T.; Kudin, K. N.; Burant, J. C.; Millam, J. M.; Iyengar, S. S.; Tomasi, J.; ; Barone, V.; Mennucci, B.; Cossi, M.; Scalmani, G.; Rega, N.; ; Petersson, G. A.; Nakatsuji, H.; Hada, M.; Ehara, M.; Toyota, K.; Fukuda, R.; Hasegawa, J.; Ishida, M.; Nakajima, T.; Honda, Y.; Kitao, O.; Nakai, H.; Klene, M.; Li, X.; Knox, J. E.; Hratchian, H. P.; Cross, J. B.; Adamo, C.; Jaramillo, J.; Gomperts, R.; Stratmann, R. E.; Yazyev, O.; Austin, A. J.; Cammi, R.; Pomelli, C.; Ochterski, J. W.; Ayala, P. Y.; Morokuma, K.; Voth, G. A.; Salvador, P.; Dannenberg, J. J.; Zakrzewski, V. G.; Dapprich, S.; Daniels, A. D.; Strain, M. C.; Farkas, O.; Malick, D. K.; Rabuck, A. D.; Raghavachari, K.; Foresman, J. B.; Ortiz, J. V.; Cui, Q.; Baboul, A. G.; Clifford, S.; Cioslowski, J.; Stefanov, B. B.; Liu, G.; Liashenko, A.; Piskorz, P.; Komaromi, I.; Martin, R. L.; Fox, D. J.; Keith, T.; Al-Laham, M. A.; Peng, C. Y.; Nanayakkara, A.; Challacombe, M.; Gill, P. M. W.; Johnson, B.; Chen, W.; Wong, M. W.; Gonzalez, C.; Pople, J. A.; *Gaussian 03*, revision E.0; Gaussian, Inc.: Wallingford, CT, 2004.
(59) *TURBOMOLE*, V6.3; Turbomole GmbH: University of Karlsruhe and Forschungszentrum Karlsruhe GmbH, 2011; pp 1989−2007.
(60) Frisch, M. J.; Trucks, G. W.; Schlegel, H. B.; Scuseria, G. E.; Robb, M. A.; Cheeseman, J. R.; Scalmani, G.; Barone, V.; Mennucci, B.; Petersson, G. A.; Nakatsuji, H.; Caricato, M.; Li, X.; Hratchian, H. P.; Izmaylov, A. F.; Bloino, J.; Zheng, G.; Sonnenberg, J. L.; Hada, M.; Ehara, M.; Toyota, K.; Fukuda, R.; Hasegawa, J.; Ishida, M.; Nakajima, T.; Honda, Y.; Kitao, O.; Nakai, H.; Vreven, T.; Montgomery, J. A., Jr.; Peralta, J. E.; Ogliaro, F.; Bearpark, M.; Heyd, J. J.; Brothers, E.; Kudin, K. N.; Staroverov, V. N.; Kobayashi, R.; Normand, J.; Raghavachari, K.; Rendell, A.; Burant, J. C.; Iyengar, S. S.; Tomasi, J.; Cossi, M.; Rega, N.; Millam, N. J.; Klene, M.; Knox, J. E.; Cross, J. B.; Bakken, V.; Adamo, C.; Jaramillo, J.; Gomperts, R.; Stratmann, R. E.; Yazyev, O.; Austin, A. J.; Cammi, R.; Pomelli, C.; Ochterski, J. W.; Martin, R. L.; Morokuma, K.; Zakrzewski, V. G.; Voth, G. A.; Salvador, P.; Dannenberg, J. J.; Dapprich, S.; Daniels, A. D.; Farkas, Ö.; Foresman, J. B.; Ortiz, J. V.; Cioslowski, J.; Fox, D. J. *Gaussian 09*, revision A.2; Gaussian, Inc.: Wallingford, CT, 2009.
(61) Klamt, A. *J. Phys. Chem.* **1995**, *99*, 2224−2235.
(62) Barone, V.; Cossi, M. *J. Phys. Chem. A* **1998**, *102*, 1995−2001.
(63) Cossi, M.; Rega, N.; Scalmani, G.; Barone, V. *J. Comput. Chem.* **2003**, *24*, 669−681.
(64) York, D. M.; Karplus, M. *J. Phys. Chem. A* **1999**, *103*, 11060−11079.
(65) Scalmani, G.; Frisch, M. J. *J. Chem. Phys.* **2010**, *132*, 114110/1−15.
(66) Klamt, A. *J. Phys. Chem.* **1996**, *100*, 3349−3353.
(67) Scalmani, G.; Frisch, M. J.; Mennucci, B.; Tomasi, J.; Cammi, R.; Barone, V. *J. Chem. Phys.* **2006**, *124*, 094107/1−15.
(68) Schäfer, A.; Horn, H.; Ahlrichs, R. *J. Chem. Phys.* **1992**, *97*, 2571−2577.
(69) Schäfer, A.; Huber, C.; Ahlrichs, R. *J. Chem. Phys.* **1994**, *100*, 5829.
(70) Becke, A. D. *Phys. Rev. A: At., Mol., Opt. Phys.* **1988**, *38*, 3098−3100.
(71) Lee, C.; Yang, W.; Parr, R. G. *Phys. Rev. B: Condens. Matter Mater. Phys.* **1988**, *37*, 785−789.
(72) Becke, A. D. *J. Chem. Phys.* **1993**, *98*, 1372−1377.
(73) Boese, A. D.; Martin, J. M. L. *J. Chem. Phys.* **2004**, *121*, 3405−3416.
(74) Zhao, Y.; Schultz, N. E.; Truhlar, D. G. *J. Chem. Phys.* **2005**, *123*, 161103/1−4.
(75) Zhao, Y.; Truhlar, D. G. *Theor. Chem. Acc.* **2008**, *120*, 215−241.

(76) Zhao, Y.; Schultz, N. E.; Truhlar, D. G. *J. Chem. Theory Comput.* **2006**, *2*, 364−382.
(77) Yanai, T.; Tew, D. P.; Handy, N. C. *Chem. Phys. Lett.* **2004**, *393*, 51−57.
(78) Chai, J. D.; Head-Gordon, M. *J. Chem. Phys.* **2008**, *128*, 084106/1−15.
(79) Iikura, H.; Tsuneda, T.; Yanai, T.; Hirao, K. *J. Chem. Phys.* **2001**, *115*, 3540−3544.
(80) Schwabe, T.; Grimme, S. *Phys. Chem. Chem. Phys.* **2007**, *9*, 3397−3406.
(81) Klamt, A.; Eckert, F.; Arlt, W. *Annu. Rev. Chem. Biomol. Eng.* **2010**, *1*, 101−122.
(82) Eckert, F.; Klamt, A. *AlChE J.* **2002**, *48*, 369−385.
(83) Eckert, F.; Klamt, A. *COSMOtherm, C2.1*, Release 01.11; COSMOlogic GmbH & Co KG: Leverkusen, Germany, 2010.
(84) Neese, F. *ORCA − an ab initio, Density Functional and Semiempirical Program Package*, Version 2.4; Max-Planck Institut für Bioanorganische Chemie: Mühlheim an der Ruhr, Germany, 2004.
(85) Plotner, J.; Tozer, D. J.; Dreuw, A. *J. Chem. Theory Comput.* **2010**, *6*, 2315−2324.
(86) Lynch, B. J.; Fast, P. L.; Harris, M.; Truhlar, D. G. *J. Phys. Chem. A* **2000**, *104*, 4811−4815.
(87) Brown, N. J.; Lancashire, H. N.; Fox, M. A.; Collison, D.; Edge, R.; Yufit, D. S.; Howard, J. A. K.; Whiteley, M. W.; Low, P. J. *Organometallics* **2011**, *30*, 884−894.
(88) Fox, M. A.; Roberts, R. L.; Baines, T. E.; Le Guennic, B.; Halet, J. F.; Hartl, F.; Yufit, D. S.; Albesa-Jove, D.; Howard, J. A. K.; Low, P. J. *J. Am. Chem. Soc.* **2008**, *130*, 3566−3578.
(89) Arbuznikov, A. V.; Bahmann, H.; Kaupp, M. *J. Phys. Chem. A* **2009**, *113*, 11898−11906.
(90) Theilacker, K.; Arbuznikov, A. V.; Bahmann, H.; Kaupp, M. *J. Phys. Chem. A* **2011**, *115*, 8990−8996.
(91) Arbuznikov, A. V.; Kaupp, M. *J. Chem. Phys.* **2012**, *136*, 014111/1−13.
(92) Reich, H. J.; Borst, J. P.; Dykstra, R. R.; Green, D. P. *J. Am. Chem. Soc.* **1993**, *115*, 8728−8741.
(93) Klamt, A.; Jonas, V.; Burger, T.; Lohrenz, J. C. W. *J. Phys. Chem. A* **1998**, *102*, 5074−5085.
(94) Klamt, A. *Ind. Eng. Chem. Res.* **2007**, *47*, 987−988.
(95) Klamt, A. *WIREs Comput. Mol. Sci.* **2011**, *1*, 699−709.

## ■ NOTE ADDED AFTER ASAP PUBLICATION

Due to a production error, this paper was published on the Web on September 14, 2012, with minor text errors. The corrected version was reposted on September 17, 2012.